ACADEMIC PRESS

Available online at www.sciencedirect.com

SCIENCE DIRECT®

Journal of Computational Physics 186 (2003) 70–92

JOURNAL OF COMPUTATIONAL PHYSICS

www.elsevier.com/locate/jcp

On the calculation of the water particle kinematics arising in a directionally spread wavefield

W.J.D. Bateman [a,1], C. Swan [a,*], P.H. Taylor [b]

[a] *Department of Civil and Environmental Engineering, Imperial College, London SW7 2BU, UK*
[b] *Department of Engineering Science, Oxford University, Oxford OX1 3PJ, UK*

Received 16 January 2002; received in revised form 14 August 2002; accepted 19 December 2002

Abstract

This paper concerns the calculation of the water particle kinematics generated by the propagation of surface gravity waves. The motivation for this work lies in recent advances in the description of the water surface elevation associated with extreme waves that are highly nonlinear and involve a spread of wave energy in both frequency and direction. To provide these exact numerical descriptions the nonlinear free-surface boundary conditions are time-marched, with the most efficient solutions simply based upon the water surface elevation, η, and the velocity potential, ϕ, on that surface. In many broad-banded problems, computational efficiency is not merely desirable but absolutely essential to resolve the complex interactions between wave components with widely varying length-scales and different directions of propagation. Although such models have recently been developed, the calculation of the underlying water particle kinematics, based on the surface properties alone, remains a significant obstacle to their practical application. The present paper tackles this problem, outlining a new method based upon an adaptation of an existing approximation to the Dirichlet–Neumann operator. This solution, which is presently formulated for flow over a flat bed, is appropriate to the description of any kinematic quantity and has the over-riding advantage that it is both stable and computationally efficient. Indeed, its only limitation arises from the assumed Fourier series representations. As a result, both η and ϕ must be single-valued functions and are not therefore appropriate to the description of overturning waves. The proposed method is compared favourably to both existing analytical wave models and laboratory data providing a description of the kinematics beneath extreme, near-breaking, waves with varying directional spread. The paper concludes by investigating two important characteristics of the flow field beneath large waves arising in realistic ocean environments.

Keywords: Water wave kinematics; Directional water waves; Extreme ocean waves; Three-dimensional wave modelling; Nonlinear wave–wave interactions; Wave groups

* Corresponding author. Tel.: +44-207-594-5999; fax: +44-207-215-2716.
E-mail addresses: will@zyba.com (W.J.D. Bateman), c.swan@ic.ac.uk (C. Swan), paul.taylor@eng.ox.ac.uk (P.H. Taylor).
[1] Present address: Risk Management Solutions Limited, 10 Eastcheap, London EC3M 1AJU.

0021-9991/03/$ - see front matter
doi:10.1016/S0021-9991(03)00012-3

1. Introduction

The accurate prediction of the water particle kinematics generated by surface water waves is an important part of any wave model. Indeed, from an engineering perspective, this information is essential since it forms the basis of force calculations on which the safe and economic design of all offshore and coastal structures rely. Although numerous wave solutions are available, the water particle kinematics associated with the largest or steepest waves arising in an ocean environment can only be predicted by models that adequately reflect the fact that such waves are transient, involving a significant spread of wave energy in both frequency and direction, and may also be highly nonlinear.

The models most appropriate to this task are based upon the numerical solution of the exact equations of motion for water waves, the Euler equations. Longuet-Higgins and Cokelet [1] first outlined the calculation procedure whereby a wavefield, initially specified in the spatial domain, could be time-marched using the nonlinear free-surface boundary conditions. Following this initial development, and based upon the same underlying methodology, several alternative solutions have sought to provide improved accuracy, stability and numerical efficiency, where the latter becomes significant when attempting to maximise the resolution appropriate to the description of steep and/or over-turning waves. With a few notable exceptions, discussed below, such models have been applied to unidirectional waves.

Broadly speaking, wave models of this type may be subdivided into two categories. The first includes models that explicitly describe the velocity potential, and hence the water particle kinematics, throughout the fluid domain. These have the advantage that the vertical derivative of the velocity potential at the water surface, necessary for the time-marching process, is easily calculated. However, they have the over-riding disadvantage of being numerically inefficient, involving large matrix inversion, with computational effort increasing with N^3, where N defines the number of surface points. Examples of this approach include Fenton and Rienecker [2], Li and Fleming [3] and Johannessen and Swan [4,5], where the latter model represents an extension of that proposed in [2] to include the effects of directional spreading. Although this model has been successfully applied to the description of a number of relatively narrow-banded laboratory test cases, the computational effort involved is such that it cannot be applied to broad-banded ocean spectra with realistic directional spreads.

The second category of solution exploits the full benefits of the time-marching procedures originally outlined by Longuet-Higgins and Cokelet [1], employing only the velocity potential on the water surface. Such solutions, which were anticipated in the work of Zakharov [6], involve a reduction in the dimensionality of the problem leading to significantly improved numerical efficiency. In the context of unidirectional waves, Dommermuth and Yue [7] provide a spectral method in which the velocity potential is described using perturbation methods, whilst Dold and Peregrine [8] employ Cauchy integral theory to provide a very accurate and stable method in which the computational effort increases with N^2. Unfortunately, with no three-dimensional equivalent of Cauchy integral theory this method cannot be extended to include the effects of directional spreading.

In contrast, Craig and Sulem [9] achieved the required dimensional reduction using a Taylor series expansion of the Dirichlet–Neumann operator, which they referred to as their G-operator. For two-dimensional problems expansions of this type can be rigorously justified using the theory of Coifman and Mayer [10]. Although the method proposed by Craig and Sulem [9] is limited to nonoverturning waves (the Fourier series description of both the water surface elevation, η, and the velocity potential, ϕ, being restricted to single valued functions of the spatial position) it has two over-riding advantages. First, the Fourier integrals that arise in the application of the G-operator can be calculated very rapidly using fast Fourier transforms, involving a computational effort proportional to $N\log_e(N)$. Secondly, although the model proposed in [9] is only applicable to unidirectional waves, the authors clearly note that this is not an inherent limitation. Indeed, Craig et al. [11] and Nicholls [12] have provided descriptions of the Dirichlet–Neumann operator for three-dimensional domains. In the latter case Nicholls [12] applied numerical continuation methods to both

two- and three-dimensional wave problems. However, the computational efficiency of this scheme is such that parallel computing power is required to resolve a small number of wave components. In contrast, Bateman et al. [13] have applied the method originally outlined by Craig and Sulem [9] and extended the solution to include the effects of directional spreading. Comparisons between this directional wave model and recent laboratory observations, also given in [13], confirm that the water surface elevation associated with highly nonlinear, directionally spread, wavefields can be accurately reproduced with modest computational effort. Furthermore, these comparisons also demonstrate that numerical efficiency was not sought for its own sake, but was essential to achieve the resolution in the wavenumber domain necessary to describe wavefields that are broad-banded in both frequency and direction.

In applying these highly efficient wave models it is clear that an additional method is required to calculate the water particle kinematics based solely on the water surface elevation, η, and the velocity potential on that surface, $\phi_{z=\eta}$. Whilst there are currently two main methods of tackling this problem, those due to Fenton and Rienecker [2] and Dold and Peregrine [8], these approaches have traditionally only been applied to unidirectional wave problems. Indeed, preliminary investigations outlined in 2 confirm that neither of these solutions are appropriate to the description of a three-dimensional flow field.

The present paper addresses this problem and, more specifically, aims to describe the water particle kinematics associated with the highly nonlinear, transient, and directionally spread surface water waves modelled by Bateman et al. [13]. Although the approach described herein is closely related to the developments originally proposed by Craig and Sulem [9] and further extended by Bateman et al. [13], it can also be applied to other periodic wave domains, where the surface values (η and $\phi_{z=\eta}$) have been calculated by an alternative numerical or analytical method, provided the water depth is constant. To tackle this problem two new operators, referred to as the H- and H_2-operators, are introduced. Although the methods associated with these are distinct, in many cases either can be used to describe the kinematics over the entire flow field, their real value becomes apparent when they are used together to describe the kinematics beneath extreme wave groups.

Section 2 commences with a brief review of the governing equations and the kinematic method originally outlined by Fenton and Rienecker [2]. An alternative approach based on Green's second identity is also discussed. In addition to illustrating the limitations of these approaches, the review also highlights some important characteristics that appear to apply to all boundary methods. The first H-operator is discussed in Section 3. This calculates a set of global constants that can be used to describe the water particle kinematics throughout the flow field. However, this is subsequently shown to be adversely effected by high-frequency wave components present in very steep wavefields. Section 4 describes an alternative method based on the H_2-operator. This approach employs the description of the water particle kinematics along any surface (initially the free surface) and transforms it onto an alternative surface. Comparisons between the numerically predicted kinematics, calculated using both the H- and H_2-operators, and available laboratory observations are given in Section 5. Having established the success of the proposed method, Section 6 investigates some interesting properties of the water particle kinematics arising beneath extreme ocean waves. Finally, Section 7 provides some concluding remarks and comments on the practical importance of the proposed scheme.

2. Spectral and boundary integral techniques

If the output from a wave model describes the water surface elevation, η, and the velocity potential on that surface, $\phi_{z=\eta}$, the existing literature provides a number of methods for calculating the underlying water particle kinematics. Unfortunately, one of the most successful methods applied to unidirectional waves, based on Cauchy integral theory [7,8], cannot be applied to a three-dimensional domain. It is therefore not relevant to the present study of directionally spread waves and will not be considered further. Two principal methods remain, the first being based upon the spectral method proposed by Fenton and Rienecker [2] and

the second the boundary integral technique involving the application of Green's second identity. Each of these methods is briefly discussed following an initial statement of the governing equations.

2.1. Governing equations

If the fluid motion generated by waves propagating on the surface of a three-dimensional water body is irrotational, a velocity potential $\phi(x,y,z,t)$ can be defined where t indicates time and (x,y,z) represent the usual Cartesian coordinates in which (x,y) defines a horizontal plane located at the mean water level and z is measured vertically upwards. The velocity vector, $\mathbf{u}=(u,v,w)$, is defined by $\mathbf{u}=\nabla\phi$, where $\nabla=(\partial_x,\partial_y,\partial_z)$. Assuming the fluid is incompressible, mass continuity is consistent with $\nabla\cdot\mathbf{u}=0$. When expressed in terms of ϕ this yields Laplace's equation

$$\nabla^2\phi=0. \tag{1}$$

This equation applies throughout the fluid domain, $\mathfrak{D}_\eta$, which is bounded by a horizontal bed at $z=-h$ and the free surface defined by $z=\eta(x,y,t)$. On these boundaries the following conditions apply

$$\partial_z\phi=0 \quad \text{on } z=-h \tag{2}$$

and

$$\partial_t\phi+\frac{1}{2}|\nabla\phi|^2+g\eta=0 \quad \text{on } z=\eta(x,y,t), \tag{3a}$$

$$\partial_t\eta+\partial_x\eta\partial_x\phi+\partial_y\eta\partial_y\phi-\partial_z\phi=0 \quad \text{on } z=\eta(x,y,t), \tag{3b}$$

where g is the gravitational acceleration. Eq. (2) denotes the fact that the horizontal bed is assumed impermeable, while Eqs. (3a) and (3b) define the dynamic and kinematic free surface boundary conditions that, respectively, require the pressure at the water surface to be constant and the fluid particles at the surface to remain there.

In many wave models, including [9,13], it is customary to represent the dependent variables ϕ and η by a Fourier series in the horizontal (x,y) plane. Adopting this approach, the wave motion will be periodic in both the x and y directions. If λ_x and λ_y define the wavelengths in the x and y directions over which the solution is assumed periodic (commonly referred to as the 'fundamental' wavelengths) it follows that $\eta(x+\lambda_x,y+\lambda_y)=\eta(x,y)$ and $\phi\big(x+\lambda_x,y+\lambda_y,z\big)=\phi(x,y,z)$. Whilst spatially periodic boundary conditions obviously provide some limitations to the wavefields that can be successfully modelled, earlier work by [5,13] has shown that they do not impact adversely on the ability to describe large transient waves, provided they are assumed to arise due to the focusing of freely propagating wave components. In the context of large ocean waves, field observations confirm that this is indeed the case [14]. To successfully model such waves two requirements must be met. First, λ_x and λ_y must be chosen to ensure that the wavefield can be adequately represented in the wavenumber domain (k,l), where k and l are the wavenumbers in the x and y directions, respectively. Within a Fourier system k and l are integer multiples of the fundamental wavenumber components $k=nk_0$ and $l=ml_0$, where $k_0=2\pi/\lambda_x$, $l_0=2\pi/\lambda_y$, and n and m are integers. Secondly, the total number of wavenumber components must be such that the calculations remain within the practical bounds of current computing capabilities. A full discussion of these and other related issues is given in [13].

At this point it is perhaps worth noting that in seeking a solution of the underlying water particle kinematics one could adopt a direct domain solution of Laplace's equation (1). However, since the starting point for the present calculations is a given solution for $\eta(x,y,t)$ and $\phi(x,y,\eta,t)$, this would be less efficient than the methods discussed below, particularly those involving the new H-operators.

2.2. The Fenton and Rienecker solver

The method proposed originally by Fenton and Rienecker [2] uses a series of sine and cosine waves to represent the water surface. In this way the problem is broken down into a set of linear contributions to the velocity potential whose behaviour is clearly understood. For a unidirectional problem the velocity potential anywhere within the wave is assumed to be

$$\phi(x,z) = \sum_{k=0}^{\infty} \alpha_k \cosh(k(z+h))\, \mathrm{e}^{\mathrm{i}kx}, \tag{4}$$

where α_k are the complex global constants that define the water particle kinematics throughout the domain. The solution for α_k is obtained by solving a series of simultaneous equations formed from the evaluation of Eq. (4) at each surface node. In matrix form, with the unknown coefficients separated from the knowns, the problem has the following form

$$\overset{k=0}{\longrightarrow}\overset{k=\infty}{\longrightarrow}\begin{bmatrix} \cdot & \cdots & \cdot \\ \vdots & \cosh(k(\eta(x)+h))e^{ikx} & \vdots \\ \cdot & \cdots & \cdot \end{bmatrix}\Bigg\downarrow{\scriptstyle x=0}^{\scriptstyle x=\lambda_x} \times \begin{bmatrix} \vdots \\ \alpha_k \\ \vdots \end{bmatrix}\Bigg\downarrow{\scriptstyle k=0}_{\scriptstyle k=\infty} = \begin{bmatrix} \vdots \\ \Phi(x) \\ \vdots \end{bmatrix}\Bigg\downarrow{\scriptstyle x=0}_{\scriptstyle x=\lambda_x}, \tag{5}$$

where $\Phi(x) = \phi(x,\eta(x))$ for a unidirectional wavefield. The values of α_k are found by multiplying Φ with the inverse of the coefficient matrix. Due to the fully populated state of the coefficient matrix, lower–upper factorisation is amongst the best methods for inverting this matrix. Unfortunately, with current computing facilities the application of this approach to most three-dimensional domains is impractical. For example, a problem with $N = 256 \times 256$ surface points, would require in excess of 1 GB of memory and take a 700 MHz Pentium III approximately two weeks to compute the inverse matrix, a process that has to be undertaken for each time-step at which kinematics data is required. Whilst it is possible to implement multigrid relaxation methods [3] to speed up the calculation, the memory requirements remain a considerable problem for realistic directionally spread problems. Obviously, computing time may be significantly reduced using a parallel implementation. However, recent work by Jakobus [15] involving an optimised lower–upper decomposition on a Cray T3E with 60 processors suggests that a similar sized problem would still take up to 20 h per time step.

In addition to the limitations imposed by the computational procedure, Vijfvinkel [16] has also shown that the method may suffer from the amplification of small numerical errors. In order to obtain the desired velocity components throughout the fluid domain ϕ, defined in Eq. (4), must be differentiated either horizontally or vertically. For example, the horizontal velocities in a unidirectional wave are given by

$$u(x,z) = \partial_x \phi(x,z) = \sum_{k=0}^{\infty} \alpha_k \mathrm{i}k \cosh(k(z+h))\, \mathrm{e}^{\mathrm{i}kx}. \tag{6}$$

The difficulties associated with this approach are considered in Fig. 1. This example concerns the depth-variation in the horizontal velocity arising beneath the crest of a regular Stokes' wave, with a steepness of $ak = 0.33$, and contrasts the results of the Fenton and Rienecker [2] method (Eq. (4)) with a fifth-order analytic Stokes' solution based on the method outlined by Fenton [17]. In this example small numerical errors, arising in the high-wavenumber range, are amplified by the differentiation process leading to erroneous velocity predictions close to the water surface.

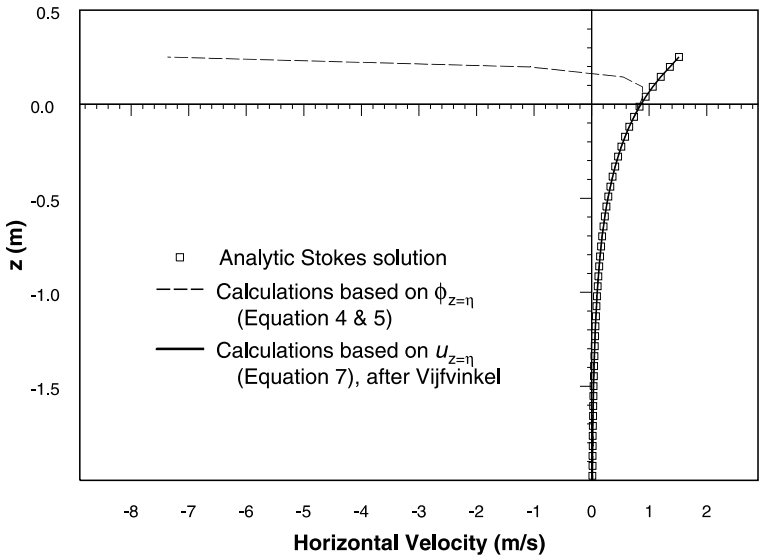

Fig. 1. The effect of high frequency errors on the horizontal velocities beneath a Stokes wave ($ak = 0.33$).

In many respects this problem is similar to the difficulties associated with high-frequency contamination, commonly experienced when a linear random wave theory is applied to the description of the kinematics beneath a large wave crest, Sobey [18]. In the present case small high-wavenumber errors, arising as a consequence of numerical rounding and/or aliasing, are amplified massively as they are extrapolated onto the water surface. Whilst it may be possible to remove these errors by filtering, there is currently no clear methodology to ensure that physically important information is not lost. Alternatively, Vijfvinkel [16] has shown that at least some of these errors may be controlled by calculating the required velocities on the free surface prior to determining the global constants. For example, applying the G-operator developed by Bateman et al. [13], the horizontal velocity on the water surface is defined by $[\partial_x \phi]_{z=\eta} = \partial_x \Phi - \partial_x \eta G(\eta)\Phi$, where $\Phi = \phi_{z=\eta}$. Using this result, an alternative set of unknown global constants, β_k, may be defined that directly describe the required kinematics

$$u(x,y,z) = \sum_{k=0}^{\infty} \beta_k \cosh(k(z+h))\, \mathrm{e}^{\mathrm{i}kx}. \tag{7}$$

Applying this method to the previous example considered in Fig. 1, the predicted horizontal velocity profile, $u(z)$, is shown to be in good agreement with the Stokes' solution [17].

Despite these difficulties, methods similar to that outlined by Fenton and Rienecker [2] have been successfully used to model a large number of unidirectional wave cases [4,16]. More recently, they have also been applied to the description of a number of simple, laboratory-scale, multi-directional problems [5]. Nevertheless, the potential difficulties in modelling realistically broad-banded sea states using this apparently straightforward approach, not least because of the restrictions imposed by its poor computational efficiency, should not be under-estimated.

2.3. Green's second identity

The advantage of the dimensional reduction arising from the exact projection of the equations of wave motion onto the water surface were noted in Section 1. In effect, any methodology that facilitates this

reduction can be applied in reverse to yield the velocity potential, and hence the water particle kinematics, at any internal point subject to known values of $\eta(x,y)$ and $\phi(x,y,\eta)$. It has also been noted that for three-dimensional domains Cauchy integral theory is inappropriate. However, Green's theory, or more specifically Green's second identity, offers a viable alternative such that

$$\phi = \int\int_S \left(\phi \frac{\partial \hat{G}}{\partial n} - \hat{G} \frac{\partial \phi}{\partial n} \right) \mathrm{d}S, \tag{8}$$

where ϕ is defined at any point within the domain, the integral is taken over the boundary S of the domain, n is the outward facing normal and $\hat{G} = 1/(4\pi R)$, where R is the radial distance from the internal point of interest to the position on the boundary.

Although, as far as the authors are aware, this method has not been specifically used to calculate the internal water particle kinematics, it has formed the basis of the dimensional reduction critical to the success of several earlier models. Examples include Longuet-Higgins and Cokelet [1] and Fenton and Mills [19] in two-dimensions and Isaacson [20] and Romate [21] in three-dimensions.

In reviewing this material the benefits of applying Green's theory are readily apparent:

(i) The methodology can be expanded to include the effects of variable bathymetry [19],
(ii) It can be applied to directional domains with nonrectangular geometries [20,22],
(iii) Unlike the Fourier based methods there is no assumed periodicity, particularly important when seeking to model waves propagating up a slope or the interaction of waves with fixed or floating structures, and
(iv) The shape of the water surface is not limited to nonoverturning waves [1].

Despite these obvious advantages it is important to note that the previous applications of Green's theory have reported significant problems with the growth of high wavenumber instabilities. These are particularly apparent in the two-dimensional calculations reported in [1,19] and in the three-dimensional studies of [21]. At this stage it is not clear whether these difficulties are a direct result of adopting the Green's theory approach or whether they arise due to the numerical approaches employed or, in some cases, because of a desire to model a more complex problem involving the interaction with fixed or floating bodies [20,22]. However, the work by Romate [21] is particularly telling in that it does not include the interaction with fixed or floating bodies but seeks to model a relatively simple unidirectional wave train within a three-dimensional domain. In this case, the only one presented, the instabilities are such that the simulation breaks down shortly after 100 time-steps, corresponding to less than a single wave period. This is in marked contrast to the preliminary results reported by Bateman et al. [13] in which they demonstrated that their three-dimensional model could successfully describe a unidirectional wave train propagating at any angle across the computational domain. Furthermore, in these and many other wave cases involving highly nonlinear, near-breaking, directionally spread wave fields, the stability of the model was such that no filtering was required.

Given the success of this latter approach it was decided to progress with the calculation of the water particle kinematics using an adaptation of the three-dimensional G-operator developed in [13]. Nevertheless, the advantages of the Green's theory approach (noted above) are significant and separate work is presently underway to investigate its effective application to the evolution of three-dimensional wavefields.

3. The H-operator

The method outlined within this section builds upon the solution originally proposed by Fenton and Rienecker [2]. In effect, the H-operator provides an alternative to the computationally intensive method proposed in [2] for calculating the global unknown constants (α_k). Specifically, it replaces the slow matrix

inversion with an approximation that can be calculated very rapidly. Due to reduced numerical rounding errors this H-operator approximation is often more accurate than results obtained using lower–upper factorisation, even though the latter method is formally 'exact'. When the operator is applied to an arbitrary kinematic quantity, ξ, at the surface of a three-dimensional domain, it calculates

$$H(\eta)\xi^S = \sum_{k=-\infty}^{\infty}\sum_{l=-\infty}^{\infty} \alpha_{kl}\sinh(Kh)\,\mathrm{e}^{\mathrm{i}(kx+ly)}, \tag{9}$$

where the superscript s denotes the value of the quantity evaluated at the water surface, $\xi^S(x,y,t) = \xi(x,y,\eta(x,y,t),t)$, α_{kl} are the global constants that describe ξ everywhere within the fluid domain and $K = \sqrt{k^2+l^2}$, where (k,l) are the wavenumbers in the x and y directions, respectively. A simple Fourier transformation of this result obtains $\alpha_{kl}\sinh(Kh)$ from which α_{kl} are isolated by dividing by the known constant $\sinh(Kh)$. It therefore follows that

$$\xi(x,y,z,t) = \sum_{k=-\infty}^{\infty}\sum_{l=-\infty}^{\infty} \alpha_{kl}\cosh(K(z+h))\,\mathrm{e}^{\mathrm{i}(kx+ly)}. \tag{10}$$

This equation is suitable for describing the variation of terms such as ϕ or $u = \phi_x$ whose profile with depth is described by the summation of cosh terms. For an alternative conjugate variable such as $w = \phi_z$ the cosh term in Eq. (10) should be replaced by a sinh. This inevitably leads to a different form for the H-operator, although the result given by the right-hand side of (9) remains unchanged.

In the remainder of this paper, the derivation appropriate for resolving kinematic profiles with a depth dependency related to cosh only is provided for both the H- and H_2-operators. In practice, however, the quantity ξ can be taken to be any linear function of the velocity potential, Φ. Accordingly, it must satisfy $\nabla^2\xi = 0$.

3.1. Derivation

For simplicity the initial equations shown in this section are for a single wavenumber component involving only one value of l and k. Following the development of the G-operator [9,13], the H-operator is defined as the sum of a Taylor series

$$H(\eta) = \sum_{m=0}^{\infty} H_m(\eta). \tag{11}$$

This operator may be applied to a general kinematic variable, representing any kinematic quantity, specified on the water surface, ξ^S. If Eq. (10) is evaluated at the water surface, $z = \eta$, and expanded about $\eta = 0$ using a Taylor expansion

$$\xi^S = \left[\sum_{\substack{j\geqslant 0\\ j\ \text{even}}} \frac{1}{j!}(K\eta)^j\cosh(Kh) + \sum_{\substack{j>0\\ j\ \text{odd}}} \frac{1}{j!}(K\eta)^j\sinh(Kh)\right]\alpha_{kl}\,\mathrm{e}^{\mathrm{i}(kx+ly)}. \tag{12}$$

This expansion moves the variable z, expressed as η, outside the cosh term and permits their rapid evaluation using Fast Fourier transforms (FFTs). Substituting Eqs. (11) and (12) into (9) and dividing throughout by $\cosh(Kh)$ gives

$$\left[\sum_{m=0}^{\infty} H_m(\eta)\right]\left[\sum_{\substack{j\geqslant 0\\ j\ \text{even}}} \frac{1}{j!}(K\eta)^j + \sum_{\substack{j>0\\ j\ \text{odd}}} \frac{1}{j!}(K\eta)^j\tanh(Kh)\right]\alpha_{kl}\,\mathrm{e}^{\mathrm{i}(kx+ly)} = \alpha_{kl}\tanh(Kh)\,\mathrm{e}^{\mathrm{i}(kx+ly)}. \tag{13}$$

To simplify this equation, the summations on the left-hand side are re-ordered using a series law

$$\sum_{m=0}^{\infty} a_m \sum_{j=0}^{\infty} b_j = \sum_{j=0}^{\infty} \left(\sum_{m=0}^{j} a_m b_{j-m} \right) \tag{14}$$

to produce a summation of homogeneous powers from which even and odd terms of the same degree can be identified.

Using Fourier analysis it may be shown that a solution appropriate to multiple components can be obtained by integrating over all wavenumber components

$$f(D)\phi^S(x,y) = \frac{1}{4\pi^2} \int\int f(K)\alpha_{kl}\, \mathrm{e}^{\mathrm{i}(kx+ly)}\, \mathrm{d}k\, \mathrm{d}l \tag{15}$$

with

$$D = -\mathrm{i}\frac{\mathrm{d}}{\mathrm{d}r} \quad \text{and} \quad \alpha_{kl} = \int\int \phi^S(x,y)\, \mathrm{e}^{-\mathrm{i}(kx+ly)}\, \mathrm{d}x\, \mathrm{d}y,$$

where D is a complex radial derivative operator in physical space, $r = \sqrt{x^2+y^2}$ and a_{kl} are the global constants found from a Fourier transform of Φ. After applying (14) and (15), the general form of (13) appropriate to multiple components can be written as:

for $j = 0$

$$H_0(\eta) = \tanh(Dh), \tag{16a}$$

for $j \geqslant 1$ and odd

$$H_j(\eta) = -\sum_{\substack{m<j \\ m\ \text{odd}}} H_m(\eta) \frac{1}{(j-m)!} (D\eta)^{j-m} - \sum_{\substack{m<j \\ m\ \text{even}}} H_m(\eta) \frac{1}{(j-m)!} (D\eta)^{j-m} \tanh(Dh), \tag{16b}$$

for $j \geqslant 2$ and even

$$H_j(\eta) = -\sum_{\substack{m<j \\ m\ \text{even}}} H_m(\eta) \frac{1}{(j-m)!} (D\eta)^{j-m} - \sum_{\substack{m<j \\ m\ \text{odd}}} H_m(\eta) \frac{1}{(j-m)!} (D\eta)^{j-m} \tanh(Dh). \tag{16c}$$

The evaluation of the operator at any arbitrary order, requires the evaluation of the operator at all previous (or lower) orders. During this process there are many instances where identical (or near identical) terms are re-evaluated. Accordingly, the computational effort required to evaluate any order of the operator above zero can be significantly improved by storing the values of previously calculated terms that are subsequently re-used. This 'improved' method may be summarised by

$$H_m(\eta)\xi^S = \tanh(Dh)\mu_m, \tag{17}$$

where

$$\mu_0 = \xi^S,$$

$$\mu_{j>0} = -\sum_{\substack{1 \leqslant n \leqslant j \\ n\ \text{even}}} \frac{\eta^n D^n[\mu_{j-n}]}{n!} - \sum_{\substack{1 \leqslant n \leqslant j \\ n\ \text{odd}}} \frac{\eta^n D^n \tanh(Dh)[\mu_{j-n}]}{n!}.$$

The solution given in (17) is derived for the case of finite water depth. In infinite depth the solution is considerably simpler, with the $\tanh(Dh)$ terms being replaced by $\mathrm{sign}(D)$.

Expanding the first three terms of this solution gives:

$$\begin{aligned} H_0 &= \tanh(Dh), \\ H_1 &= -\tanh(Dh)\eta D\tanh(Dh), \\ H_2 &= -\frac{1}{2}\tanh(Dh)\eta^2 D^2 + \tanh(Dh)\eta D\tanh(Dh)\eta D\tanh(Dh). \end{aligned} \tag{18}$$

3.2. Implementation and validation

The convergence of the H-operator occurs rapidly, so that in the majority of cases it is sufficient to evaluate the first ten terms in the series expansion. To validate this expansion the operator was applied to the analytic surface parameters from a unidirectional regular wave train. With the input specified by the surface parameters (η and Φ) from an analytical Stokes' solution [17], the global constants defining the internal kinematics are all accurately recovered. To illustrate this, Fig. 2, shows the inline horizontal velocities beneath the crests of three regular wave systems. Each set of calculations was performed in a fully three-dimensional computational domain, with the unidirectional waves propagating at 0°, 20° and 45° to the x-axis. In each case the surface parameters have been prescribed using a fifth-order Stokes solution [17]. Comparisons between these results and the analytical solution for the horizontal velocity beneath a wave crest, $u_{\mathrm{crest}}(z)$, are provided. These results confirm that the H-operator is capable of recovering the global constants, α_{kl}, required to describe the variation of $u(x,y,z)$. To avoid points obscuring each other, alternate results are shown from each of the three directions. In these, and several other preliminary cases, the differences between the theoretical Stokes' solution and the predicted kinematics are small. For example, for the cases considered on Fig. 2 the variations in the surface velocities are: $u_{\mathrm{Stokes}} = 0.901$ m/s, $u_{0^\circ} = 0.903$ m/s, $u_{20^\circ} = 0.899$ m/s, and $u_{45^\circ} = 0.899$ m/s, representing a maximum error of 0.2%.

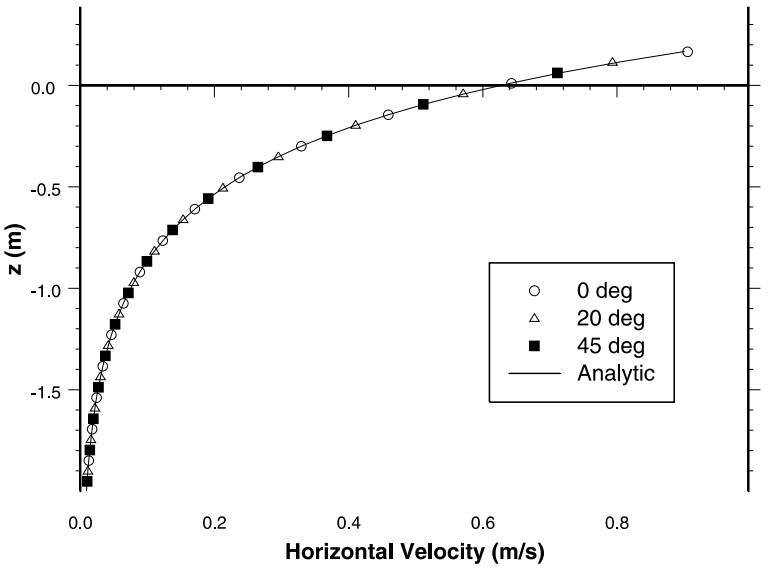

Fig. 2. A comparison between the horizontal velocities calculated from a simulation of steady Stokes waves ($ak = 0.3$) at different angles across a numerical domain $N = 128 \times 128$.

Although these results are encouraging, further preliminary investigations have shown that the H-operator can become divergent when applied to problems involving substantially different length-scales. A process similar to 'high-frequency contamination', Sobey [18], produces errors in the predicted kinematics close to the water surface. This appears to be related to the convergence of the Taylor series (11) which is reduced for very high wavenumber terms as the deviation of the water surface from the mean water level increases. As a result, the most significant errors arise during the calculation of the kinematics profile beneath the crest of an extreme wave. Unfortunately, from an engineering perspective, this corresponds to an area of particular interest.

An example of this problem is highlighted on Figs. 3 and 4. These results concern a steep focused wave group first investigated in a laboratory study by Baldock et al. [23] (case Bud55, Figure 5c, p. 659) and subsequently considered by Bateman et al. [13]. This wavefield is unidirectional and the underlying frequency spectrum relatively broad-banded. In the present example, the surface parameters (η and Φ) have been generated using the method proposed by Dold and Peregrine [8]. Using this approach, which is widely regarded as being both computationally efficient and highly accurate, the solution has inadvertently generated noise in the high wavenumber regime. Evidence of this is given in Fig. 3(a) which describes the wavenumber spectrum, $S_{\eta\eta}(k)$, derived from a spatial description of the water surface elevation at the instant of wave focusing. Although this noise is extremely small (note the logarithmic vertical scale) and should therefore have no practical impact on the water particle kinematics, it adversely effects the velocities calculated using the H-operator such that large errors arise close to the water surface. Direct evidence of this is given in Fig. 4 which concerns the horizontal velocities arising beneath the largest, or focused, wave crest. Within this figure the exact surface velocity, calculated using the G-operator proposed in [13], is indicated by the open square. Comparison between this value and the predictions based on the H-operator

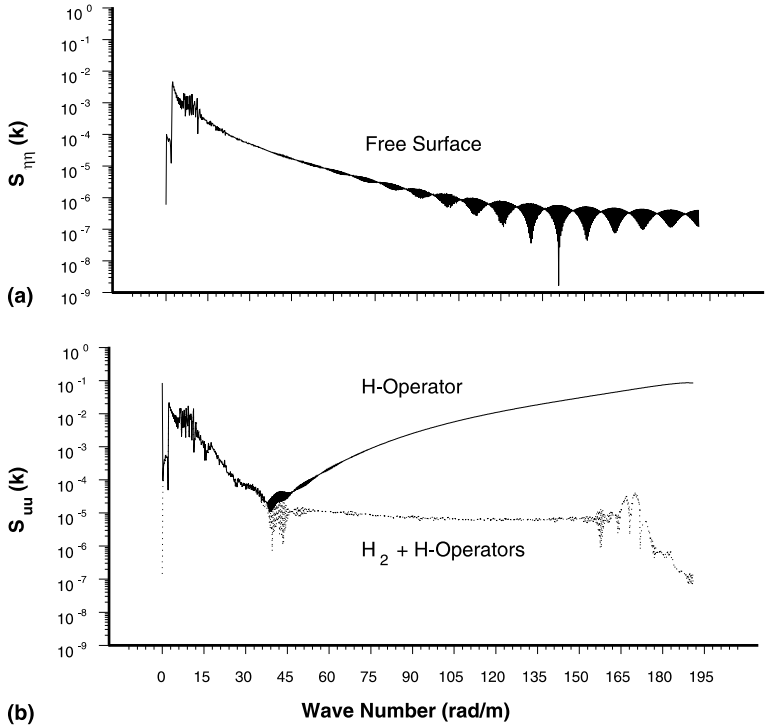

Fig. 3. Spectral distributions of: (a) water surface elevation; (b) horizontal velocity.

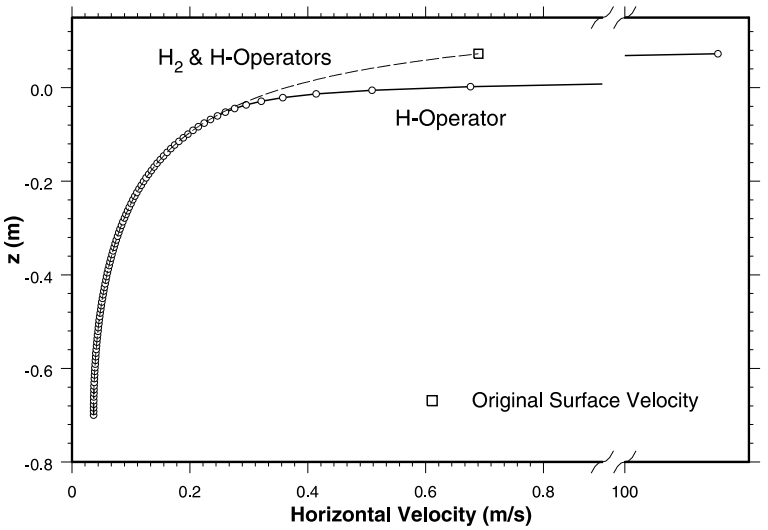

Fig. 4. The difference between the H- and H_2-operators, when used to calculate the horizontal velocities beneath the crest of a strongly nonlinear wave (case B with A = 55 mm). Note the break in the x-axis.

confirms that the latter involves a very large over-prediction of the near-surface velocities. Further evidence of this is given in Fig. 3(b). This describes a spectrum, in wavenumber space, based upon a spatial description of the horizontal water particle velocity arising on the water surface at the instant of wave focusing, $S_{uu}(k)$. The errors associated with the H-operator are clearly apparent, with significant and spurious distributions arising in the high wavenumber components.

In hindsight, difficulties of this type might have been anticipated. Unlike the three-dimensional G-operator [13], for which no evidence of nonconvergence was found, the H-operator transforms values of the kinematic variable, ξ, from $z = \eta$ to $z = 0$ in a single step. If the crest elevations are large and ξ involves contributions from very large wavenumber components, the rate of change of ξ will be rapid. This is exactly the situation in which the Taylor series might be expected to become divergent. Recent work by Nicholls and Reitich [24,25] provides important insights into the stability of perturbation methods for the evaluation of Dirichlet–Neumann operators, highlighting the potential sensitivity of these methods to the amplification of round-off errors. Although this work specifically relates to the G-operators developed in [9,13], it also has implications for the stability of the H-operator given its related derivation.

4. The H_2-operator

To overcome the problems encountered with the first H-operator, a second operator (H_2) has been developed which allows the kinematic values on any surface to be transformed onto a second arbitrary surface. If this operator transforms the arbitrary kinematic quantity, ξ, from an initial surface η onto a new surface η_2, the following definition applies

$$H_2(\eta, \eta_2)\xi(x, y, \eta) = \xi(x, y, \eta_2). \tag{19}$$

Introducing Eq. (10), the H_2-operator is given by

$$H_2(\eta)\xi(x, y, \eta) = \sum_{k=-\infty}^{\infty} \sum_{l=-\infty}^{\infty} \alpha_{kl} \cosh(K(\eta_2 + h))\, \mathrm{e}^{\mathrm{i}(kx+ly)}. \tag{20}$$

Provided the vertical distance between η and η_2 is not excessively large, the convergence of the operator is maintained. At this point it is important to note that the convergence of both the H- and the H_2-operators has not been investigated in a rigorous mathematical sense. Nevertheless, extensive numerical calculations have shown that the operators are convergent when applied according to the limitations adopted herein. Further discussion of this are given in Sections 4.2, 4.3, and 5.

4.1. Derivation

The steps associated with the formal derivation of this operator are virtually identical to the derivation of the H-operator given above and also the three-dimensional G-operator detailed in [13]. Avoiding repetition, the basic solution for H_2 in water of finite depth is given by:

for $m \geqslant 0$ and even

$$H_{2_m}(\eta,\eta_2) = \frac{1}{m!}(\eta_2 D)^m - \sum_{\substack{n<m \\ m \text{ even}}} H_{2_n}(\eta)\frac{1}{(m-n)!}(\eta D)^{m-n} - \sum_{\substack{n<m \\ m \text{ odd}}} H_{2_n}(\eta)\frac{1}{(m-n)!}(\eta D)^{m-n} \tanh(Dh), \tag{21a}$$

for $m \geqslant 1$ and odd

$$H_{2_m}(\eta,\eta_2) = \frac{1}{m!}(\eta_2 D)^m \tanh(Dh) - \sum_{\substack{n<m \\ m \text{ odd}}} H_{2_n}(\eta)\frac{1}{(m-n)!}(\eta D)^{m-n} - \sum_{\substack{n<m \\ m \text{ even}}} H_{2_n}(\eta)\frac{1}{(m-n)}(\eta D)^{m-n} \tan(Dh). \tag{21b}$$

In accordance with the previous solutions, the definition of the H_2-operator appropriate to infinite water depths is simply acquired by replacing the $\tanh(Dh)$ terms with $\mathrm{sign}(D)$. Given that the H_2-operator will typically be applied several times in a series of successive calculations (see below), there are considerable benefits in forming a 'quick' version, similar to that outlined for the H-operator (17). After undertaking a similar analysis of the order of calculations involved, an improved solution can be defined accordingly

$$H_{2_m}(\eta,\eta_2)\xi(x,y,\eta) = \sum_{\substack{n<m \\ m-n \text{ even}}} \eta_2^{m-n}\frac{1}{(m-n)!}D^{m-n}[\mu_n] + \sum_{\substack{n<m \\ m-n \text{ odd}}} \eta_2^{m-n}\frac{1}{(m-n)!}D^{m-n}\tanh(Dh)[\mu_n] - \mu_m, \tag{22}$$

where

$$\mu_0 = \xi^S,$$

$$\mu_j = \sum_{\substack{n<j \\ j-n \text{ even}}} \eta_2^{j-n}\frac{1}{(j-n)!}D^{j-n}[\mu_n] + \sum_{\substack{n<j \\ j-n \text{ odd}}} \eta_2^{j-n}\frac{1}{(j-n)!}D^{j-n}\tanh(Dh)[\mu_n].$$

Expanding this solution gives:

$$\begin{aligned} H_{2_0} &= 1, \\ H_{2_1} &= \eta_2 D\tanh(Dh) - \eta D\tanh(Dh), \\ H_{2_2} &= \frac{1}{2}\eta_2^2 D^2 - \frac{1}{2}\eta^2 D^2 - \eta_2 D\tanh(Dh)\eta_2 D\tanh(Dh) + \eta D\tanh(Dh)\eta D\tanh(Dh). \end{aligned} \tag{23}$$

The fact that the operator is equal to unity when $\eta = \eta_2$ follows directly from the definition given in (19).

4.2. Implementation

The H_2-operator becomes particularly important when seeking to calculate kinematic profiles for steep waves with a wide spectral bandwidth ($k_{\max} > 50k_{\min}$). For less steep, narrow-banded problems the original H-operator, outlined in Section 3, can be applied without modification. However, as the wave steepness and underlying spectral bandwidth increases, this method becomes rapidly unreliable. Indeed, the first evidence of errors, similar to those noted on Fig. 3, may arise at wavenumbers as small as five times that of the spectral peak.

Although, in theory, the H_2-operator can be used to calculate the kinematics at any point within the wave domain (given sufficient iterations) its use becomes increasingly cumbersome and subject to large errors when it is required to calculate the kinematics far beneath the water surface. A more logical approach is to apply the two operators sequentially, building upon their respective strengths, thereby avoiding both the difficulties associated with numerical accuracy and the over-prediction of near-surface values relating to 'high-frequency' contamination.

In the first part of this approach the H_2-operator is used to gradually transform $\xi(x, y, \eta)$ onto increasingly flatter surfaces, i.e. $\eta_2 = c \times \eta$, where c reduces from one down to zero. The size of the increments with which c is reduced must be linked to the initial steepness of the wave profile. However, in all cases investigated to date, no more that ten steps were needed to yield the required results. This choice is important since too many steps will magnify the numerical errors (although they remain very small), while too few steps will cause convergence problems similar to those identified with the original H-operator. Once the kinematic values have been transformed to a suitable elevation (typically $(\partial_x \eta)_{\max} < 0.1$), the H-operator can be applied to calculate the global constants, from which the kinematics anywhere can be evaluated. It is perhaps worthwhile to note that if the final application of the H_2-operator transforms the kinematics onto a flat surface, *say* $\eta_2 = 0$, the zero term of the H-operator is sufficient to make the final calculations.

The only difficulties with this calculation procedure concerns the possible existence of the singularities identified by McIver and Peregrine [26]. These arise in an analytical extension of the flow field above the free surface. If, in applying $\eta_2 = c\eta$, this imaginary representation of the water surface passes through these singularities, the solution may break down. So far, no problems of this type have been encountered. Nevertheless, a simple procedure to avoid such difficulties is to create an imaginary reference level that is at least as low as the lowest trough. The surface elevation can then be redefined to be $\eta_{\text{new}} = \eta_{\text{initial}} + \text{offset}$,

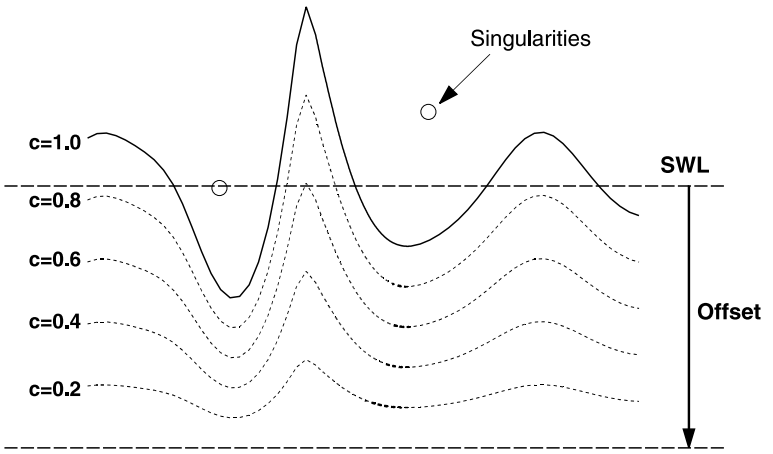

Fig. 5. The possible position of singularities and an example of the gradual reduction of the surface onto an *offset* horizontal plane.

with the depth to still water level defined as $h_{\text{new}} = h_{\text{initial}} - \text{offset}$. The process of calculating the velocities then proceeds as before, but in this shifted plane of reference. When the kinematics are transformed to a new (and perhaps flat) plane, this imaginary surface will always be within the bounds of the original fluid domain ($\mathfrak{D}_\eta$). Fig. 5 describes the application of this procedure, with successively smaller values of c used in each application of the H_2-operator.

4.3. Validation

Returning to the previous example (Case Bud55), the dashed line on Fig. 4 shows an alternative solution for $u(z)$ based on the use of both the H and H_2 operators as described above. Whilst some high-wave-number noise remains (Fig. 3(b)), the size of this is too small to have any noticeable effect. Using this new approach, the velocities calculated from the global constants produce a solution whose surface values are within 0.1% of the values originally known at the water surface.

5. Comparisons to laboratory data

The laboratory data provided by Johannessen and Swan [27] allows further rigorous assessment of the methodology used to determine the water particle kinematics. This experimental study provides detailed measurements of a large number of focused wave groups involving a spread of energy in both frequency and direction. Moreover, the study includes several sets of wave kinematics measurements for cases that were observed to be within 4% (in terms of the input amplitudes) of the limit at which incipient wave breaking was first observed. Such waves are highly nonlinear and provide an excellent example of wave conditions for which accurate predictions of the associated water particle kinematics are both practically important and notoriously difficult. Within the laboratory study three underlying frequency spectra, $S_{\eta\eta}(w)$, were considered: case B was relatively broad-banded, case D narrow-banded and case C intermediate. In each of these cases, six different directional spreads were considered corresponding to $s = \infty$ (or unidirectional), $s = 150$, 45, 25, 10 and 4, where s is the Mitsyasu [28] spreading parameter. For each combination of frequency spectra, $S_{\eta\eta}(w)$, and directional spread, s, a range of input amplitudes, A, were considered, where A defines the linear sum of the component wave amplitudes $A = \sum_{n=1}^{N} a_n$, a_n is the amplitude of the nth wave component and N is the total number of wave components. Given the nature of the focusing event, A also corresponds to the linearly predicted crest elevation at the focal position.

To distinguish between the various test cases, the notation devised by [27] and adopted in [13], will also be applied herein. Accordingly, specific test cases are referred to by their input frequency spectrum, their linear or input amplitude sum and their directional spread. For example, case B66s45 corresponds to the broad-banded frequency spectra (case B), an input amplitude of $A = 66$ mm, and a directional spread of $s = 45$. The description and implementation of these parameters to generate a numerical simulation of the evolving water surface is detailed in [13]. Using the values of η and Φ from these earlier calculations, $u_{z=\eta}$ is calculated using the G-operator,

$$u_{z=\eta} = \partial_x \Phi - \partial_x \eta G(\eta)[\Phi]. \tag{24}$$

From this result repeated applications of the H_2-operator allows the horizontal velocities to be calculated at the still water level ($z = 0$), after which the H-operator is applied to determine the global kinematic constants. Finally Eq. (7) is used to produce profiles of the horizontal velocity with depth.

Figs. 6(a)–(f) concern the horizontal velocity profiles, $u(z)$, recorded beneath the largest wave crest ($x = 0$ m and $t = 0$ s) corresponding to six highly nonlinear focused wave groups. The six cases concern both broad- and narrow-banded frequency spectra (cases B and D) and involve a range of directional spreads from $s = \infty$ (a unidirectional wave denoted by 'ud'), directionally spread but relatively long crested waves

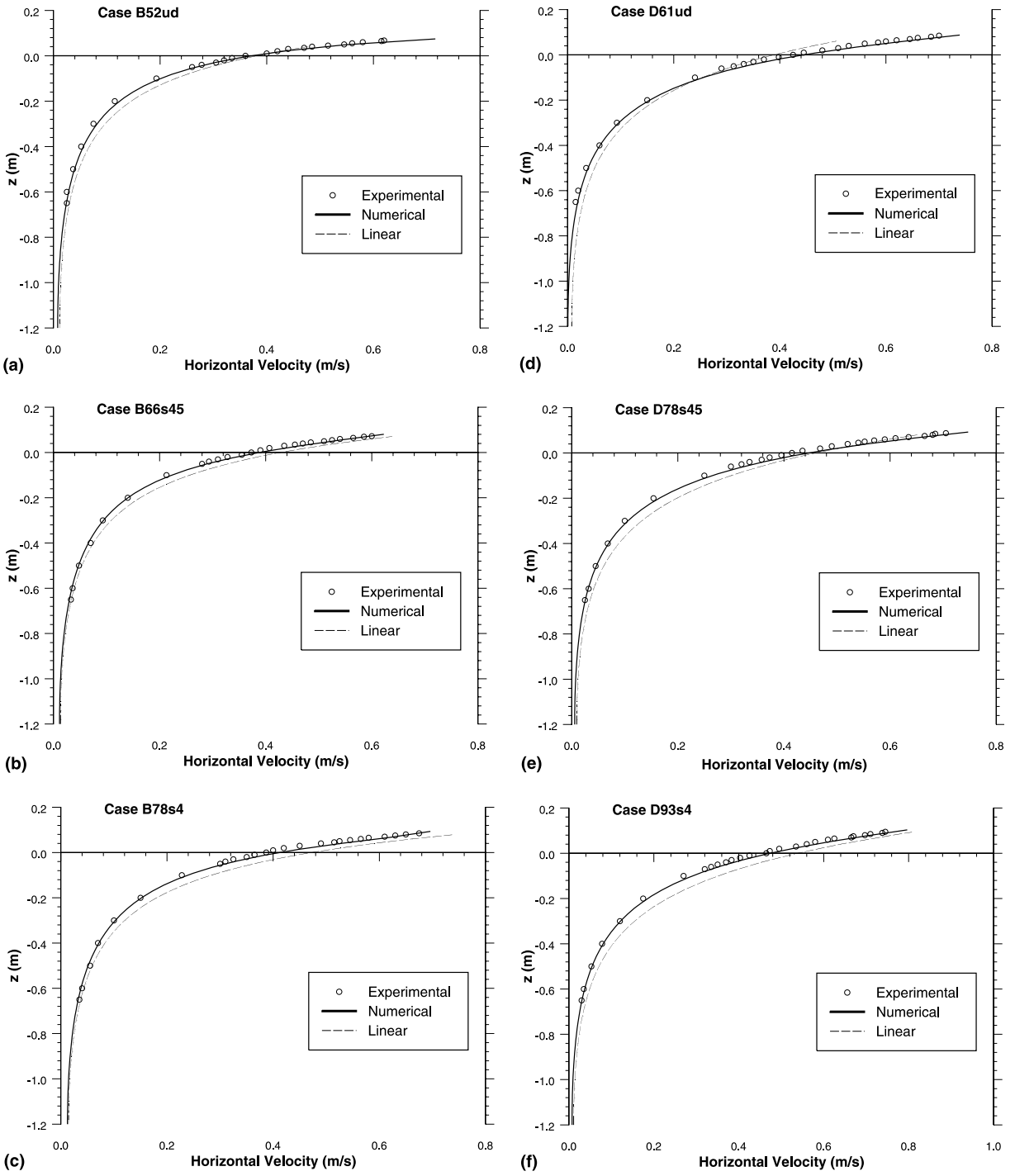

Fig. 6. Horizontal velocities, $u(z)$, at the focal time ($t = 0$) and the focal position ($x = 0$), for unidirectional and directionally spread waves. (a)–(c) are broad-banded spectrum, case B and (d)–(f) are narrow-banded spectrum, case D.

corresponding to $s = 45$, and very short-crested waves with a large directional spread corresponding to $s = 4$. In each case the numerical approximations are shown to be in very good agreement with the laboratory data. There are, however, two small differences:

(i) The numerical predictions typically show a small over-estimate of the experimental data at all depths. Detailed analysis of the evolving wavefields suggest that this may be accounted for by small inconsistencies between the numerical predictions and the laboratory observations, specifically concerning the spatial location to which the velocity data relates. In the numerical predictions the calculated velocities correspond to the behaviour directly beneath the largest wave crest. In the laboratory study the discrete spacing of the wave gauges, at 100 mm intervals, means that it is not possible to achieve a corresponding level of precision and consequently one would expect to record slightly lower velocities. Nevertheless, the largest over-estimate is less than 2%, which corresponds closely to the measurement accuracy of the laser Doppler anemometer employed by Johannessen and Swan [27].

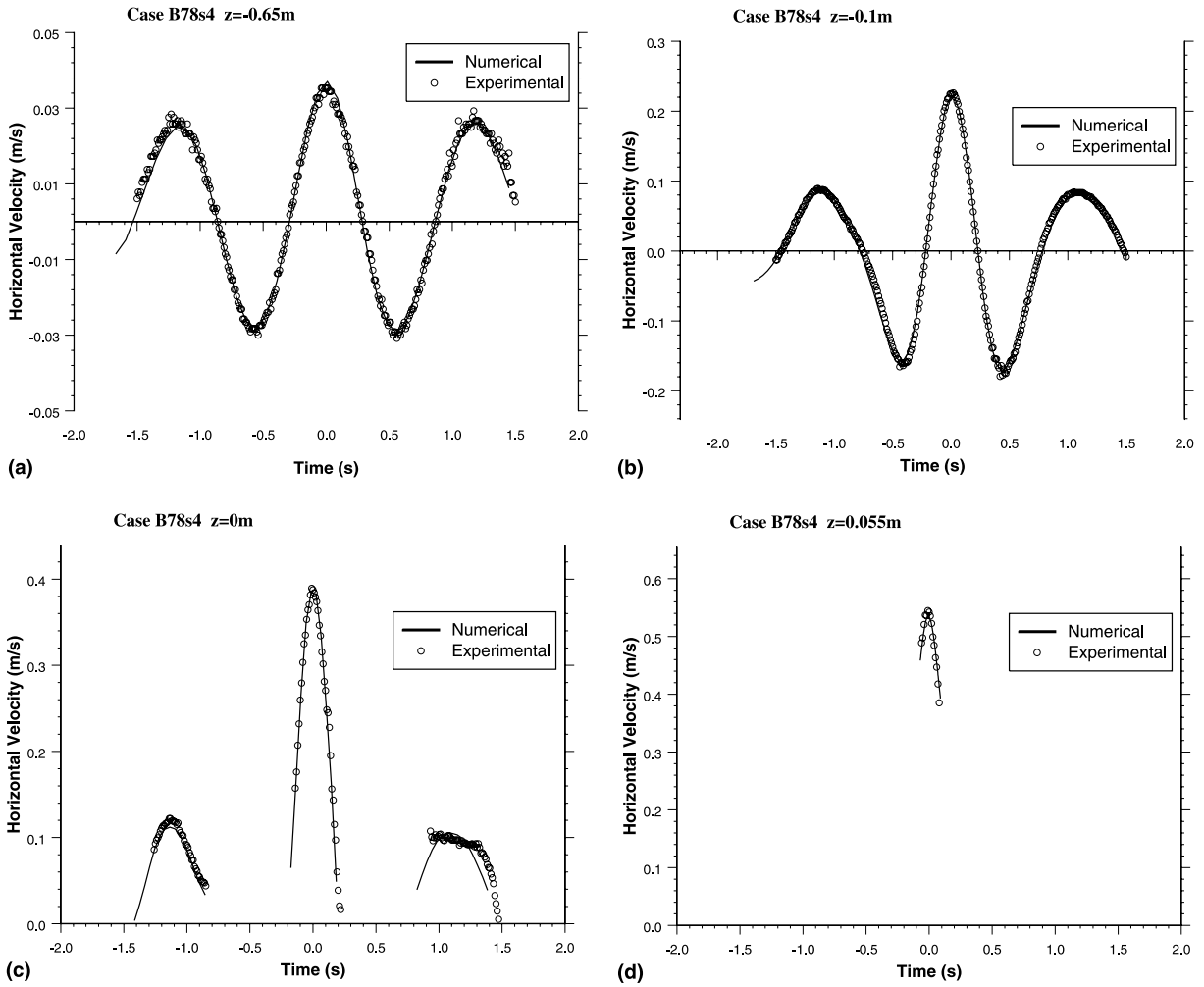

Fig. 7. Temporal profiles of the horizontal velocity, $u(t)$, at specific elevations, z, for case D93s4: (a) $z = -0.65$ m, (b) $z = -0.1$ m, (c) $z = 0$ m (SWL), (d) $z = 0.055$ m.

(ii) The largest numerical velocities exceed those measured experimentally. Again this is to be expected since it is impossible to measure velocities at the limit of a wave crest that only exists for a very small fraction of a second. Indeed, Johannessen and Swan [27] note that they were only able to measure the horizontal velocities to within 4–6 mm of the maximum crest elevation. Although this is very good from an experimental perspective, it accounts for the slight discrepancies that appear at the top of each of the velocity profiles.

To further validate the proposed methodology, Fig. 7 concerns case D93s4 and provides time-histories of the x-component of the horizontal water particle velocity, u, recorded at four elevations. In parts (a) and (b) the elevations ($z = -0.65$ and -0.1 m, respectively) lie beneath the level of the deepest wave trough and consequently the velocity traces are continuous. In contrast, parts (c) and (d) concern elevations ($z = -0.0$ m and -0.055 m, respectively) that lie within the crest-trough region. As a result, the corresponding velocity traces are intermittent. Indeed, in part (d) the elevation is such that only a brief section of velocity data is recovered, corresponding to the passage of the largest wave crest. At each of these four elevations the predicted water particle kinematics, based upon the combined application of the H- and H_2-operators, are shown to be in good agreement with the laboratory data provided by Johannessen and Swan [27].

At this point it is perhaps important to note that the agreement between the numerical and experimental results presented on Figs. 6 and 7 is further verification of numerical time-stepping scheme proposed by Bateman et al. [13]. Without the precise description of the surface parameters (η and Φ) provided by this model, the accurate prediction of the associated water particle kinematics would have been impossible, irrespective of the accuracy of the two H-operators.

6. Kinematics predictions beneath extreme ocean waves

The success of the H-operators when compared to the experimental results presented in 5 illustrate that the new method for calculating the water particle kinematics is both accurate and stable. Furthermore, the computational efficiency of these operators allows the first realistic opportunity to predict accurate, fully nonlinear, representations of the water particle kinematics beneath extreme ocean waves, characterised by a significant spread of energy in both frequency and direction. In the absence of field data describing the kinematics beneath such waves, particularly close to the water surface, direct comparisons with the present procedures are not possible. Nevertheless, the new methodology can be used to investigate some interesting features of the kinematics arising beneath extreme ocean waves.

6.1. Horizontal velocities

Within this subsection we will re-consider the numerical wave case generated earlier by Bateman et al. [13] (see their Figure 10, p. 302). This case is important since it represents the first fully nonlinear simulation of a typical design wave appropriate to the northern North Sea. The specific case chosen represents a 1 in 10,000 year event, for which the underlying frequency spectrum is based upon a JONSWAP spectrum with a peak period of $T_p = 13.5$ s and a peak enhancement factor of $\gamma = 1.7$. The wave height is defined as $H = 25$ m, the water depth is assumed deep and the directional spread is given by a Mitsuyasu [28] distribution with $s = 7$. This directional spread corresponds closely to a normal distribution with a standard deviation of $\sigma_\theta = 30^\circ$, which is consistent with the field observations of Jonathan and Taylor [14].

Numerically generated kinematics data relating to this extreme, directionally spread, wave case are presented on Fig. 8. Fully nonlinear calculations of this type are both practically relevant and were not previously possible without recourse to some form of local Fourier approximation, the best example of which is provided by Barker and Sobey [29]. Although this latter model is undoubtedly useful, particularly when describing the kinematics beneath a measured wave profile, there is some uncertainty concerning its

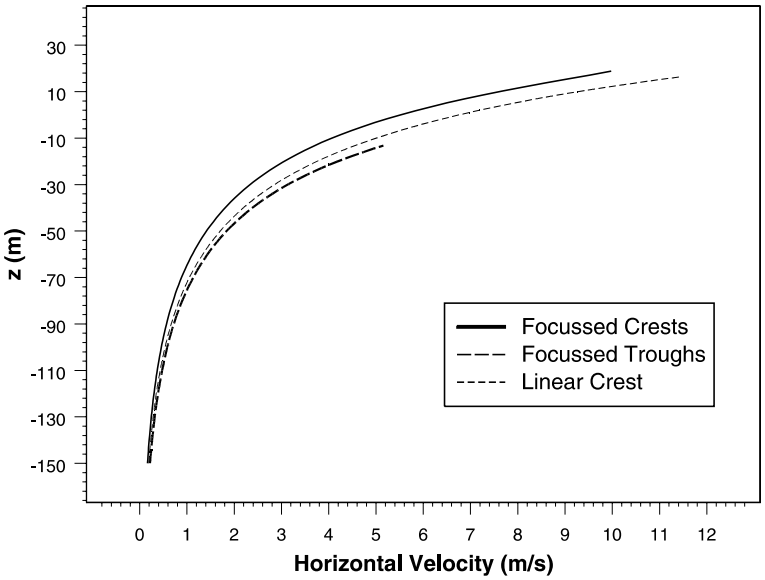

Fig. 8. The horizontal velocity profile beneath a focussed crest and trough.

ability to describe certain features of the flow field, particularly the maximum water particle acceleration and the set-down beneath a large wave group [30].

The data presented on Fig. 8 has two purposes. First, it describes the depth-variation in the maximum horizontal velocities arising directly beneath the largest or focused wave crest. Whilst it is obviously important to reiterate that there are no field data with which to validate the numerical predictions, the general form of the velocity distributions is consistent with expectations (including its departure from linear theory). Given the agreement with laboratory data achieved in 5 there would appear to be no reason to doubt the accuracy of these results.

Secondly, Fig. 8 also provides comparisons with the horizontal velocities arising beneath a focused wave trough generated in an identical wavefield. This latter case is produced in exactly the same manner as the focused crest case, the only difference being that the initial conditions specified at $t = t_0$ are inverted so that $\eta^{\mathrm{t}}(x, y, t_0) = -\eta^{\mathrm{c}}(x, y, t_0)$, where the superscripts 't' and 'c' denote the trough and crest focused cases, respectively. To illustrate the difference in these velocity distributions, Fig. 8 contrasts the positive velocities arising beneath the focused crest case with the magnitude of the negative velocities arising beneath the focused trough case. These results clearly indicate that for elevations that are permanently submerged (beneath the level of the deepest wave trough) the negative velocities beneath a wave trough are significantly larger than the positive velocities beneath a wave crest.

A physical explanation for this lies in the set-down beneath the wave group. At second-order, $\mathrm{O}(a^2k^2)$, this corresponds to the well-established wavenumber-difference terms [31]. These produce a negative or 'return' flow that decays gradually with depth due to the small wavenumbers involved. Such effects are dependent upon the envelope of the wave group and are therefore largely independent of whether the group involves focused crests or focused troughs [5,23]. In the two cases presented on Fig. 8, the 'return' flow will act to reduce the positive velocities beneath the wave crest, but will add to the magnitude of the negative velocities arising beneath the wave trough. Although this change is not unexpected, the magnitude of the effect noted in Fig. 8 is perhaps surprising. Indeed, from a practical perspective it suggests that in the design of a fully submerged structure or structural member, lying beneath the level of the deepest wave trough, the drag forces arising beneath a focused trough should be considered in preference to a focused crest. From a

statistical perspective, the crest and trough focused cases are equally likely to occur. As a result, the neglect of the increased fluid velocities arising in the latter case potentially represents an important failure in some design calculations.

6.2. Vertical accelerations

Longuet-Higgins [32] first postulated the existence of sub-surface vertical accelerations that are larger in magnitude than the values arising at the water surface. This section provides verification of this using

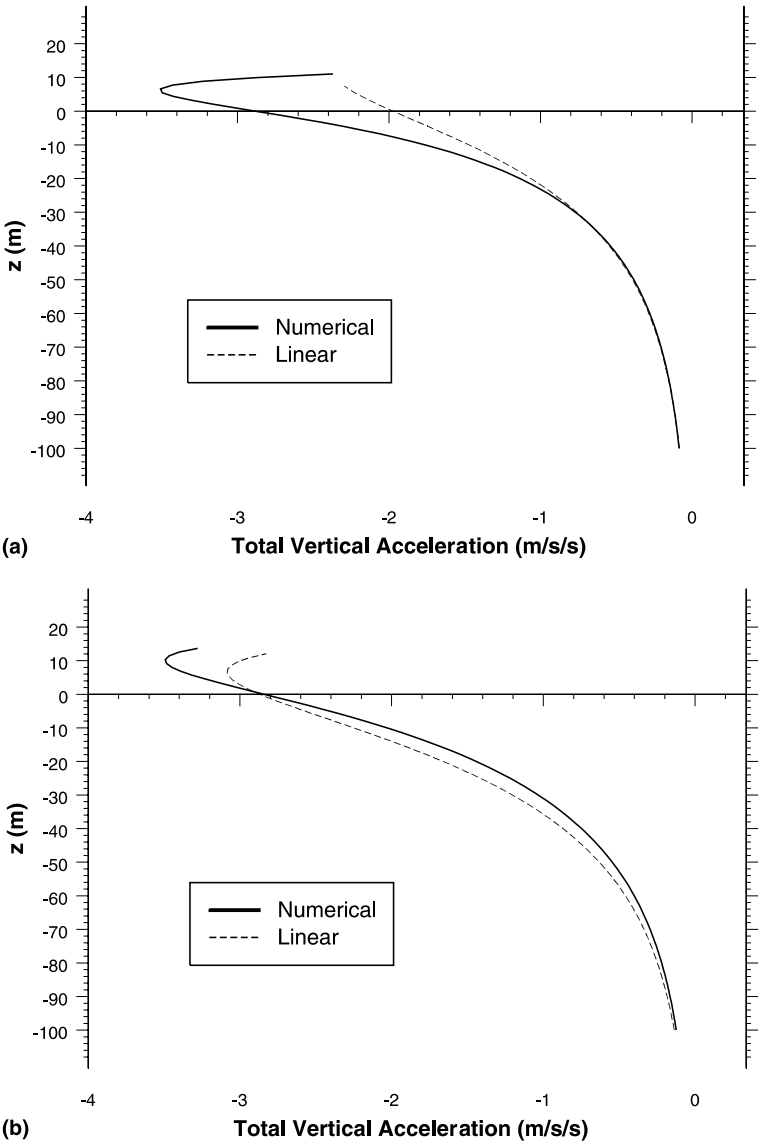

Fig. 9. Profiles of the total vertical acceleration beneath extreme water waves: (a) in a unidirectional wavefield; (b) in a directionally spread wavefield.

results from two deep water wave cases: one unidirectional and other directional. The chosen wave cases both correspond to the focusing of wave crests and have a spread of energy in the frequency domain characterised by a JONSWAP spectrum with a peak period of $T_p = 11.4$ s and a peak enhancement factor of $\gamma = 3$. The wave height is defined by $H = 18.4$ m and the directionally spread case has a Mitsuyasu [28] spreading parameter of $s = 7$ or ($\sigma_\theta = 30^\circ$).

To investigate the depth-variation in the total vertical water particle acceleration (both steady and convective) values of this parameter must first be defined on the water surface. With the total vertical acceleration defined by

$$\mathrm{d}_t w = \partial_t w + u\partial_x w + v\partial_y w + w\partial_z w, \tag{25}$$

it follows from the earlier definition of the G-operator [13] that

$$[\mathrm{d}_t w]_{z=\eta} = G(\eta)[\partial_t \Phi] + [\partial_x \phi]_{z=\eta} G(\eta)[\partial_z \Phi] - [\partial_z \phi]_{z=\eta}(\partial_{xx}\Phi - \partial_x \eta G(\eta)[\partial_x \Phi]). \tag{26}$$

Within this equation values of $\partial_t \Phi$ are calculated from the dynamic boundary condition (3b), $[\partial_z \phi]_{z=\eta} = G(\eta)\Phi$, $\partial_x \Phi$ is defined from the Fourier differentiation of Φ, and $[\partial_x \phi]_{z=\eta} = \partial_x \Phi - \partial_x \eta\, G(\eta)\Phi$. Further information concerning the calculation of these terms is given in [33].

Having defined the surface values, they are transformed to the still water level, $\eta = 0$, using the H_2-operator (4) and then the H-operator (3a) and (3b) is applied to define the global constants. The results of this process are presented on Fig. 9, with the data describing the depth-variation in the total vertical acceleration (25) arising directly beneath a focused wave crest. The figure concerns both unidirectional (Fig. 9(a)) and multi-directional (Fig. 9(b)) wave cases and contrasts the fully nonlinear calculations with the results of linear wave theory. These comparisons are important in two respects. First, they confirm the earlier work of Longuet-Higgins [32] in that the maximum magnitude of the vertical accelerations clearly arise at some distance beneath the water surface. Secondly, they are of practical significance since it is common practice in both coastal and ocean engineering to determine the properties of a surface wavefield based upon data from accelerometers located on surface-riding wave buoys. If a linear wave theory is used to calculate the wave properties, as is commonly the case, it is clear from the comparisons provided on Fig. 9 that significant errors may result.

7. Concluding remarks

This paper has considered the description of the water particle kinematics beneath both unidirectional and multi-directional surface water waves. The proposed methodology only requires information on the surface of the wave, $\eta(x,y)$ and $\phi(x,y,\eta)$, and is capable of predicting the kinematics associated with the steepest, near-breaking, waves. In combination, the H- and H_2-operators are not merely accurate and computationally efficient, but allow the solution of problems that could not otherwise be tackled using previously available methods. For example, Cauchy integral theory cannot be implemented in three-dimensions, while lower–upper factorisation requires excessive levels of memory and computing power when tackling realistic three-dimensional domains. This is particularly relevant to the description of the water particle kinematics generated by large ocean waves, involving a significant spread of energy in both frequency and direction.

The most significant limitation of the proposed model arises because both the water surface elevation, $\eta(x,y)$, and the prescribed kinematics on that surface, $\xi(x,y,\eta)$, are represented as Fourier series. It therefore follows that both η and ξ are single-valued functions that are periodic in each of the horizontal coordinate directions (x,y). This single-valued criteria restricts the applicability of the model to nonoverturning waves. Furthermore, the assumed periodicity is necessary to ensure that the spatial derivatives can

be evaluated rapidly using fast Fourier transforms. This latter requirement is not necessarily physically realistic but is, nonetheless, essential since it allows a large range of length-scales, commonly associated with realistic ocean waves, to be included in each co-ordinate direction.

The proposed method has been validated against existing analytical theories and, perhaps more importantly, against recent laboratory data describing extreme, near-breaking, waves in a directionally spread sea. In both cases the level of agreement is good. Although the present scheme can be combined with any wave model capable of describing $\eta(x, y)$ and $\xi(x, y, \eta)$, subject to the limitations noted above, the potential benefits are best realised when it is used in conjunction with the three-dimensional *G*-operator described previously by Bateman et al. [13]. If these two methods are taken together, they provide a complete and fully nonlinear solution capable of describing the characteristics of extreme ocean waves with relatively modest computational effort. The results of such calculations are relevant to the design of both offshore and coastal structures and are particularly important given the growing evidence of their susceptibility to very large waves.

References

[1] M.S. Longuet-Higgins, E.D. Cokelet, The deformation of steep surface waves on water. A numerical method of computation, Proc. R. Soc. Ser. A 350 (1976) 1–26.
[2] J.D. Fenton, M.M. Rienecker, A Fourier method for solving nonlinear water-wave problems: application to solitary-wave interactions, J. Fluid Mech. 118 (1982) 411–443.
[3] B. Li, C.A. Fleming, A three-dimensional multigrid model for fully nonlinear water waves, Coast. Eng. 30 (1997) 235–258.
[4] T.B. Johannessen, C. Swan, Nonlinear transient water waves – Part 1. A numerical method of computation with comparisons to 2-D laboratory data, Appl. Ocean Res. 19 (1997) 293–308.
[5] T.B. Johannessen, C. Swan, The nonlinear dynamics of focused wave groups in two and three dimensions, Proc. R. Soc. Ser. A, 2003 (in press).
[6] V. Zakharov, Stability of periodic waves of finite amplitude on the surface of a deep fluid, J. Appl. Mech. Tech. Phys. 9 (1968) 86–94.
[7] D.G. Dommermuth, D.K.P. Yue, Numerical simulation of nonlinear axisymmetric flows with a free surface, J. Fluid Mech. 178 (1987) 195–219.
[8] J.W. Dold, D.H. Peregrine, Steep unsteady waves: an efficient computational scheme, in: Proc. 19th Int. Conf. Coast. Eng., ASCE, 1, 1984, pp. 90–115.
[9] W. Craig, C. Sulem, Numerical simulation of gravity waves, J. Comp. Phys. 108 (1993) 73–83.
[10] R.R. Coifman, Y. Meyer, Nonlinear harmonic analysis and analytic dependence, Proc. Symp. Pure Math. 43 (1985) 71–78.
[11] W. Craig, U. Schanz, C. Sulem, The modulation limit of three-dimensional water waves, and the Davey–Stewartson system, Annales de. 1'IHP: Analyse Nonlineaire 14 (1997) 615–667.
[12] D.P. Nicholls, Traveling water waves: spectral continuation methods with parallel implementation, J. Comp. Phys. 143 (1998) 224–240.
[13] W.J.D. Bateman, C. Swan, P.H. Taylor, On the efficient numerical simulation of directionally-spread surface water waves, J. Comp. Phys. 174 (2001) 277–305.
[14] P. Jonathan, P.H. Taylor, Irregular nonlinear waves in a spread sea, ASME Trans. J. Offshore Mech. Arctic Eng. 119 (1996) 37–41.
[15] U. Jakobus, Parallel computation of electromagnetic fields based on integral equations, in: E. Krause, W. Jäger (Eds.), High Performance Computing in Science and Engineering. Transactions of the High Performance Computing Centre, Stuttgart (HLRS), Springer, Berlin, 1999, pp. 377–386.
[16] E.M. Vijfvinkel, Focused wave groups on deep and shallow water, MSc Thesis, University of Groningen, The Netherlands, 1996.
[17] J.D. Fenton, A fifth order Stokes' theory for steady waves, J. Waterways, Port, Coast. Eng. 1 (1985) 216–234.
[18] R.J. Sobey, Wave theory predictions of crest kinematics, in: O.T. Torum, Gudmestad (Eds.), Water Wave Kinematics, NATO ASI Series E: Applied Sciences, vol. 178, Kluwer Academic Publishers, Dordrecht, 1990.
[19] J.D. Fenton, D.A. Mills, Shoaling waves: numerical solution of exact equations, in: D.G. Provis, R. Radok (Eds.), Waves on Water of Variable Depth, Lecture Notes in Physics, vol. 64, Springer, Berlin, 1976, pp. 94–101.
[20] M. Isaacson, Nonlinear-wave effects on fixed and floating bodies, J. Fluid Mech. 120 (1982) 267–281.
[21] J.E. Romate, The numerical simulation of nonlinear gravity waves, Eng. Anal. Bound. Elem. 7 (4) (1990) 00. 156–166.
[22] M. Isaacson, K.F. Cheung, Time-domain second-order wave diffraction in three dimensions, J. Waterways, Port, Coast. Ocean Eng. (ASCE) 118 (5) (1992) 496–516.

[23] T.E. Baldock, C. Swan, P.H. Taylor, A laboratory study of non-linear surface waves on water, Phil. Trans. R. Soc. Lond. Ser. A 354 (1996) 649–676.
[24] D.P. Nicholls, F. Reitich, A new approach to analyticity of Dirichlet–Neumann operators, Proc. R. Soc. A Edinburgh 131 (6) (2001) 1411–1433.
[25] D.P. Nicholls, F. Reitich, Stability of high-order perturbative methods for the computation of Dirichlet–Neumann operators, J. Comp. Phys. 170 (2001) 276–298.
[26] P. McIver, D.H. Peregrine, Motion of a free surface and its representation by singularities, Bristol University Report, 1981 (unpublished).
[27] T.B. Johannessen, C. Swan, A laboratory study of the focusing of transient and directionally spread surface water waves, Proc. R. Soc. Ser. A 457 (2001) 1–36.
[28] H. Mitsuyasu, Observation of directional spectrum of ocean waves using a cloverleaf buoy, J. Phys. Oceanogr. 16 (1975) 459–482.
[29] C.H. Barker, R.J. Sobey, Directional irregular wave kinematics, Tech. Report CHL-98-24, US Army Corps of Engineers, Waterways Experiment Station, Vicksburg, MS, September 1998, 175pp.
[30] S. Smith, C. Swan, Extreme two-dimensional water waves: an assessment of potential design solutions, Ocean Eng. 29 (2002) 387–416.
[31] M.S. Longuet-Higgins, R.W. Stewart, Changes in the form of short gravity waves on long waves and tidal currents, J. Fluid Mech. 8 (1960) 565–583.
[32] M.S. Longuet-Higgins, Eulerian and Lagrangian aspects of surface waves, J. Fluid Mech. 173 (1986) 683–707.
[33] W.J.D. Bateman, A numerical investigation of three dimensional extreme water waves, PhD Thesis, Imperial College, University of London, 2000.